51. C. R. A. Catlow, C. M. Freeman, B. Vessal, S. M. Tomlinson, M. Leslie, *J. Chem. Soc., Faraday Trans.* **1991**, *87*, 1947.
52. S. Kirckpatrick, C. D. Gelatt, M. P. Vecchi, *Science* **1983**, *220*, 671.
53. T. J. H. Vlugt, M. Schenk, *J. Phys. Chem. B* **2002**, *106*, 12757.
54. P. Demontis, G. B. Suffritti, S. Quartieri, E. S. Fois, A. Gamba, *J. Phys. Chem.* **1988**, *92*, 867.
55. R. Q. Snurr, A. T. Bell, D. N. Theodorou, *J. Phys. Chem.* **1994**, *98*, 11948.
56. T. R. Forester, W. Smith, *J. Chem. Soc., Faraday Trans.* **1997**, *93*, 3249.
57. F. Leroy, B. Rousseau, A. H. Fuchs, *Phys. Chem. Chem. Phys.* **2004**, *6*, 775.
58. R. A. Jackson, C. R. A. Catlow, *Mol. Simul.* **1988**, *1*, 207.
59. T. Yamazaki, K. Masahiro, O. Sentaro, O. Yoshisada, *Mol. Phys.* **1993**, *80*, 313.
60. J. G. Harris, K. H. Yung, *J. Phys. Chem.* **1995**, *99*, 12021.
61. U. Müller, H. Reichert, E. Robens, K. K. Unger, Y. Grillet, F. Rouquerol, J. Rouquerol, P. Donfgeng, A. Mersmann, *Fresenius' Z. Anal. Chem.* **1989**, *333*, 433.
62. C. S. Murthy, K. Singer, M. L Klein, I. R. McDonald, *Mol. Phys.* **1980**, *41*, 1387.
63. R. L. June, A. T. Bell, D. N. Theodorou, *J. Phys. Chem.* **1990**, *94*, 1508.
64. B. Smit, T. L. M. Maesen, *Nature* **1995**, *374*, 42.
65. P. Pascual, A. Boutin, P. Ungerer, B. Tavitian, A. H. Fuchs, *Mol. Simul.* **2004**, *30*, 593.
66. K. M. A. De Meyer, S. Chempath, J. F. M. Denayer, J. A. Martens, R. Q. Snurr, G. Baron, *J. Phys. Chem. B* **2003**, *107*, 10760.
67. C. E. Ramachandran, S. Chempath, L. J. Broadbelt, R. Q. Snurr, *Micropor. Mesopor. Mater.* **2006**, *90*, 293.
68. E. J. Maginn, A. T. Bell, D. N. Theodorou, *J. Phys. Chem.* **1995**, *99*, 2057.
69. D. Dubbeldam, S. Calero, T. L. M. Maesen, B. Smit, *Angew. Chem. Int. Ed.* **2003**, *42*, 3624.
70. M. Schenk, S. L. Vidal, T. J. H. Vlugt, B. Smit, R. Krishna, *Langmuir* **2001**, *17*, 1558.
71. R. Krishna, S. Calero, B. Smit, *Chem. Eng. J.* **2002**, *88*, 81.
72. S. Chempath, R. Q. Snurr, J. J. Low, *AIChE J.* **2004**, *50*, 463.
73. A. L. Myers, J. M. Prausnitz, *AIChE J.* **1965**, *11*, 121.
74. E. J. Maginn, A. T. Bell, D. N. Theodorou, *J. Phys. Chem.* **1996**, *100*, 7155.
75. E. Beerdsen, B. Smit, D. Dubbeldam, *Phys. Rev. Lett.* **2004**, *93*, 248301.
76. E. J. Maginn, A. T. Bell, D. N. Theodorou, *J. Phys. Chem.* **1993**, *97*, 4173.
77. G. S. Heffelfinger, F. van Swol, *J. Chem. Phys.* **1994**, *100*, 7548.
78. G. K. Papadopoulos, *Mol. Simul.* **2005**, *31*, 57.
79. G. Arya, H. C. Chang, E. J. Maginn, *J. Chem. Phys.* **2001**, *115*, 8112.
80. A. I. Skoulidas, D. S. Sholl, *J. Phys. Chem. B.* **2002**, *106*, 5058.
81. A. I. Skoulidas, D. S. Sholl, R. Krishna, *Langmuir* **2003**, *19*, 7977.
82. A. I. Skoulidas, D. M. Ackerman, J. K. Johnson, D. S. Sholl, *Phys. Rev. Lett.* **2002**, *89*, 185901.
83. G. K. Papadopoulos, H. Jobic, D. N. Theodorou, *J. Phys. Chem. B* **2004**, *108*, 12748.
84. R. Fowler, E. A. Guggenheim, *Statistical Thermodynamics*, University Press, Cambridge, 1949, p. 421
85. D. A. Reed, G. Ehrlich, *Surf. Sci.* **1981**, *102*, 588.
86. L. N. Gergidis, D. N. Theodorou, H. Jobic, *J. Phys. Chem. B* **2000**, *104*, 5541.
87. S.-S. Chong, H. Jobic, M. Plazanet, D. S. Sholl, *Chem. Phys. Lett.* **2005**, *408*, 157.
88. R. Krishna, *Chem. Eng. J.* **2001**, *84*, 207.
89. R. Q. Snurr, J. Kärger, *J. Phys. Chem. B* **1997**, *101*, 6469.
90. S. Jost, N. K. Bar, S. Fritzsche, R. Haberlandt, J. Kärger, *J. Phys. Chem. B* **1998**, *102*, 6375.
91. L. N. Gergidis, D. N. Theodorou, *J. Phys. Chem. B* **1999**, *103*, 3380.
92. H. Jobic, D. N. Theodorou, *J. Phys. Chem. B* **2006**, *110*, 1964.
93. H. Jobic, W. Schmidt, C. B. Krause, J. Kärger, *Micropor. Mesopor. Mater.* **2006**, *90*, 299.
94. J. P. Hoogenboom, H. L. Tepper, N. F. A van der Vegt, W. J. Briels, *J. Chem. Phys.* **2000**, *113*, 6875.
95. H. L. Tepper, W. J. Briels, *J. Chem. Phys.* **2002**, *116*, 9464.
96. Y. Yan, M. E. Davis, G. R. Gavalas, *Ind. Eng. Chem. Res.* **1995**, *34*, 1652.
97. K. Kusakabe, S. Sakamoto, S. Toshiyuki, S. Morooka, *Separ. Purif. Technol.* **1999**, *16*, 139.
98. G. K. Papadopoulos, D. N. Theodorou, S. Vasenkov, J. Kärger, *J. Chem. Phys.* **2007**, *126*, 094702.
99. R. E. Cunningham, R. J. J. Williams, *Diffusion in Gases and Porous Media*, Plenum Press, New York, 1980, p. 10.
100. S. Vasenkov, W. Böhlmann, P. Galvosas, O. Geier, H. Liu, J. Kärger, *J. Phys. Chem. B* **2001**, *105*, 5922.
101. O. Geier, S. Vasenkov, E. Lehmann, J. Kärger, U. Schemmert, R. Rakoczy, J. Weitkamp, *J. Phys. Chem. B* **2001**, *105*, 10217.

5.5.3
Computer Simulations of Shape Selectivity Effects

Berend Smit and Theo M. Maesen*

5.5.3.1 Introduction

Today, almost every gasoline molecule has seen the interior of a zeolite and experienced the effect of shape selectivity. Given the economical importance [1–5] implied by this statement, one would expect that we have a very good understanding of the mechanisms underlying shape selectivity. Clearly, we do have a very good understanding of the chemical reactions that take place inside the pores of a zeolite. In addition, many mechanisms have been proposed to explain the various product distributions that have been observed experimentally. However, we are still very far away that by looking at a zeolite structure we can provide a prediction of the products.

Let us consider as a simple example the conversion of *n*-decane in an acid zeolite. The chemistry tells us that isomerization reactions take place giving mono-, di-, and tribranched isomers. These isomerization reactions compete with cracking, and this results in a large number

* Corresponding author.

of different types of shorter alkanes. Whereas the reactant is a simple linear *n*-alkane, the product is a complex distribution of many different components. So, the principle aim is to use shape selectivity in such a way that the optimal product distribution for a given application can be obtained. What should the appearance of the zeolite be in order to obtain as much dibranched products as possible? Can one envision a structure that selectively removes C_5 from the product distribution? Answering these questions requires a molecular understanding of shape selectivity, the various forms of which are reviewed in this chapter.

Weisz and Frilette coined the term ''shape selective catalysis'' during the 1950s, when they discovered that only molecules permeable into an LTA-type zeolite were catalytically converted, to the exclusion of others [6–9]. In a 1971 review Venuto pointed out that, in addition to shape selectivity, there are ''... reactions on external surfaces and special effects'' [10]. Whereas progress has been made in establishing and understanding *external surface reactions* [11–14] (variously called ''nest effects'' [15] or ''pore mouth'' [10, 11, 16–18] and ''key-lock'' [19–22] catalysis), the (other) ''special effects'' have mushroomed into a myriad of phenomena each with their individual name. An early example of these special effects is the ''window'' or ''cage effect'', coined by Chen et al. [10, 23]. However, this was later merged into the classical shape selectivity model – initially as a form of mass transport shape selectivity [23–25] and more recently as a form of sorption shape selectivity [26]. Santilli and Zones coined the term ''secondary shape selectivity'' to describe the selective hydroconversion of *n*-C_6 instead of *n*-C_{16} by AFX-type zeolites [27]. Derouane postulated that ''molecular traffic control'' might occur when small molecules can diffuse through small and large molecules through large channels of one and the same molecular sieve [28, 29]. Van Nostrand and coworkers coined the term ''inverse shape selectivity'' to denote the accelerated formation rate of reaction intermediates that have a shape more commensurate with the framework topology than others [30–32].

At this point, is it important to note that most of these mechanisms have been proposed with very little knowledge on the thermodynamics and diffusion properties of the adsorbed molecules. Molecular simulations have provided us with such thermodynamic and transport data on well-defined model systems. Here, we demonstrate that the availability of these thermodynamic data has given us new insights into the mechanism of shape selectivity.

5.5.3.2 Conventional Hydroconversion Mechanisms

Before addressing the effect of shape selectivity on these reactions, it is worthwhile first to discuss what occurs in the absence of shape selectivity.

5.5.3.2.1 Basic Mechanism

In alkane hydroconversion, a metal site dehydrogenates alkanes into alkenes, an acid site converts the alkenes into isomers or cracking products, whereupon the metal site hydrogenates the converted alkenes back into alkanes [33–35]. When starting with an *n*-alkane, the hydroconversion can be described as a series of consecutive hydroisomerization steps, with each step increasing the degree of branching [35–37]. If this process is simplified by only considering methyl group branches, the hydroisomerization of an *n*-alkane of N carbon atoms can be described as in Fig. 1. In

References see page 1690

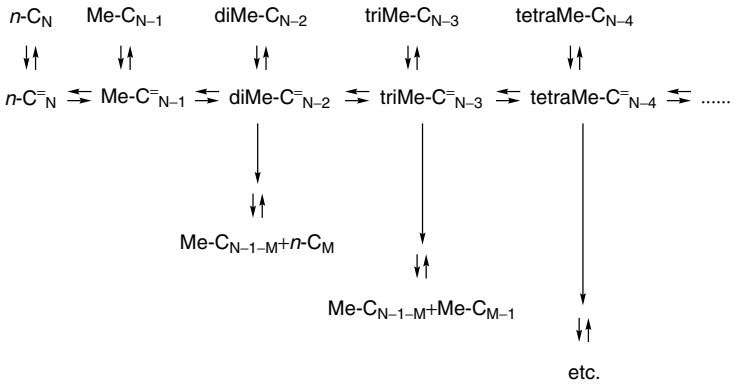

Fig. 1 Schematic reaction mechanism of an *n*-alkane hydroconversion reaction on, for example, an amorphous aluminosilicate (i.e., in the absence of shape selectivity.) *n*-Alkane feed and hydroisomerization products (top) dehydrogenate into alkene intermediates (vertical $\leftrightarrows$, e.g., Pt-catalyzed). Alkenes hydroisomerize in a chain of acid-catalyzed hydroisomerization reactions (horizontal $\leftrightarrows$). With increasing degree of branching it is increasingly more likely that isomers crack (vertical $\rightarrow$, acid-catalyzed) and hydrogenate into smaller alkanes (vertical $\leftrightarrows$, e.g., Pt-catalyzed).

addition to the hydroisomerization reactions that change the degree of branching, there are also those that change the distribution of branching towards thermodynamic equilibrium [21, 38–40]. None of the hydroisomerization reactions equilibrates completely because they compete with consecutive hydrocracking reactions that decompose the isomers [21, 36, 38–42]. The probability of a molecule undergoing a hydrocracking reaction increases with increasing degree of branching, because more extensively branched isomers afford the formation of more stable carbocationic hydrocracking transition states [21, 37–40].

For as long as the molecules are adsorbed, we refer to them as *reaction intermediates*, and they can either desorb to become a product or continue to react. Those intermediates that have two or more methyl groups sufficiently close to each other such that they can hydrocrack relatively fast, are termed *cracking precursors*. Figure 1 also illustrates that, even in an ideal hydroconversion experiment in which a single component is utilized as feed, the product is a complex mixture of products that originate from the hydroisomerizing and hydrocracking of reaction intermediates. Shape selectivity is used to optimize the product distribution for a given application.

To illustrate the type of product distribution to be expected in the absence of shape selectivity, let us consider the hydroconversion reaction of an *n*-alkane in more detail. Figure 1 suggests that the hydroisomerization reactions allow the formation of any branched isomers. At high and intermediate alkene coverage of the acid sites α, α, γ-trimethylalkene hydrocracking dominates the hydrocracking product slate [26]. When this is the case, the product slate consists of a histogram with a single maximum indicative of preferential hydrocracking at the center of the chain irrespective of the *n*-alkane feed length [26, 34–36, 43, 44]. This is because the probability of formation of α, α, γ-trimethylalkene hydrocracking precursors is dependent on the proximity of the methyl groups to the center of the chain [26, 34, 36, 37, 43]; for reasons of symmetry there are fewer permutations of their precursor transition state closer to the center [26]. For the system shown in Fig. 1 we can therefore expect a product distribution dominated by products originating from 3,3,5-trimethylheptane, and from 3,5- and 3,3- and 4,4-dimethyloctane (see Fig. 2).

In addition to the traditional kinetic *n*-alkane hydroconversion network discussed here, an alternative network was proposed [32]. Both networks agree with the older literature [45, 46] in that the cationic dialkylcyclopropyl transition states play a key role in hydroisomerization, but they disagree as to the role of these transition states in hydrocracking. The traditional network postulates that the dialkylcyclopropyl transition states only play a role in hydroisomerization, and that they have to open and form a fully fledged branched alkene before hydrocracking occurs [36, 37]. The alternative network postulates that the dialkylcyclopropyl transition states do not have to open before hydrocracking sets in, and that they themselves can initiate molecular scission [32]. Both kinetic networks are equally suitable for explaining

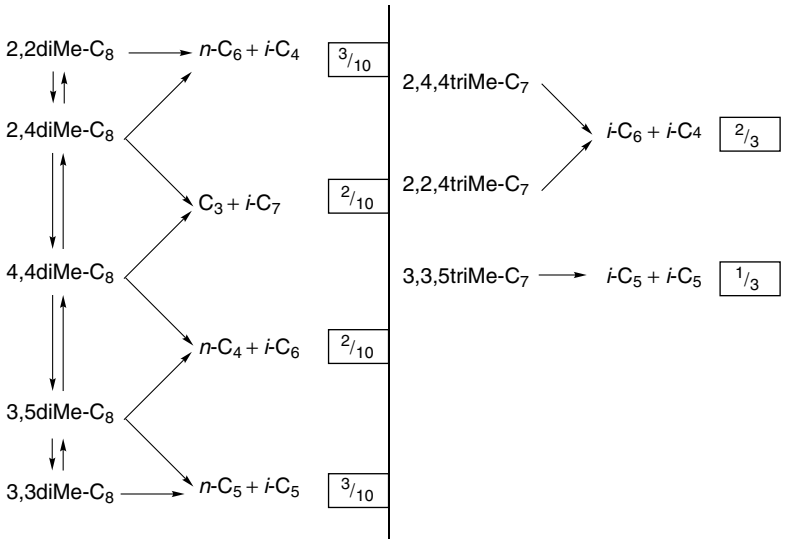

Fig. 2 The hydrocracking precursors and products of C_{10}. The boxes contain the probabilities for forming hydrocracking products, assuming that all α, γ- and α, α-dimethyloctanes are available in equal amounts and that there is no preference for hydrocracking. The same was done for α, α, γ-trimethylheptane hydrocracking. Only hydrocracking routes involving at least one tertiary carbocation transition state are included because only these routes are fast enough to make an impact. When there are only secondary carbocation transition states involved (as in monomethylalkane hydrocracking), hydrocracking occurs at a significantly lower rate.

the hydrocracking product distributions when α,α,γ-trimethylalkanes or α,γ- and α,α-dimethylalkanes dominate and the hydrocracking product slates resemble Gaussian or flat histograms [32, 37]. Here, we use the traditional network as the starting point.

5.5.3.2.2 **Shape Selectivity: General Principles** The original notion of *shape selectivity* [26] is simply the observation that, if a molecule cannot permeate through the pores of a zeolite, it will not adsorb as a reactant or desorb as a product [6]. If the adsorption of a molecule is inhibited, it will show up intact in the product slate. If the desorption of a molecule is inhibited, it could still form as a reaction intermediate in the adsorbed phase, but only molecules that originate from this reaction intermediate through consecutive reactions will show up in the product distribution. For example, the FAU-type topology exhibits large cavities in which di- and tribranched hydrocarbons form easily, whereas the TON-type topology exhibits much smaller pores in which only the monobranched isomers form easily. As a consequence, if we use the reaction scheme in Fig. 1, we deduce that the product distribution obtained from TON-type zeolites comprises many monobranched (and some dibranched) isomers and their hydrocracking products, whereas the distribution obtained from FAU-type zeolites comprises many dibranched (and some tribranched) isomers and their hydrocracking products [16]. Clearly, differently sized and shaped zeolite pores will interact differently with differently sized reactants, reaction intermediates and products. As a result, the zeolite topology can leave its ''signature'' on a particular product distribution.

Although the original concept of shape selectivity is appealingly simple, it can only explain relatively few product distributions. Therefore, forms of shape selectivity other than the originally proposed reactant and product shape selectivity have been proposed. Examples include transition state, reaction intermediate, and exterior surface shape selectivity. In the following we will provide a short discussion on these five forms of shape selectivity. In particular, the reaction scheme shown in Fig. 1 will be used to illustrate how these various forms of shape selectivity influence product distribution.

A Transition-State Shape Selectivity Transition-state shape selectivity occurs when a zeolite topology influences the reaction rates of the adsorbed molecules by modifying the relative Gibbs free energies of formation of the corresponding transition states [47, 48] (see Fig. 3). It is the only form of shape selectivity that occurs irrespective of the extent of mass transfer limitations between gas and adsorbed phase [14]. In the reaction scheme of Fig. 1, the transition state for hydroisomerization is a dialkylcyclopropyl cation. An example of transition-state selectivity is the inability of TON-type zeolites to form (and hydrocrack) α,α-dimethylalkanes [49–51]. Since the transition states in alkane hydroisomerization occur late in the reaction path, the transition state is sterically similar to the α,α-dimethylalkane products [49–51], and similar van der Waals forces will similarly increase the Gibbs free energy of formation of both the transition states and the products [52]. This linear relationship between the Gibbs free energy of formation of transition states and that of products is an example of the semi-empirical Brønsted–Evans–Polanyi (BEP) relationship [52–54]. According to this relationship, the prohibitively high Gibbs free energy of formation (and adsorption) of α,α-dimethylalkane products inside TON-type zeolites [49–51, 55] is an indication for a similarly high Gibbs free energy of formation of the transition state for α,α-dimethylalkane formation, so that transition-state shape selectivity will inhibit α,α-dimethylalkane product formation inside TON-type zeolite channels, irrespective of the absence or presence of mass transfer limitations [56].

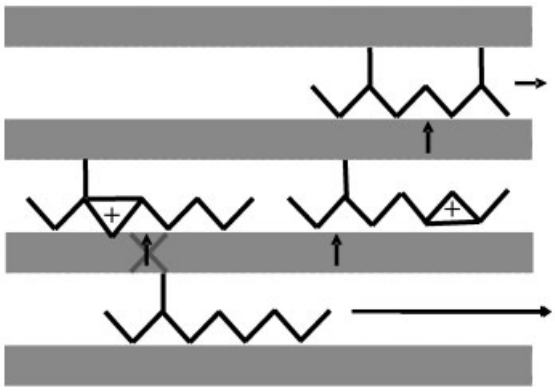

Fig. 3 Transition-state (top) and reaction-intermediate shape selectivity (bottom). In transition-state selectivity the zeolite modifies the ease of formation of a reaction intermediate by modifying the ease of generation of the transition state required for its formation; in reaction-intermediate shape selectivity the zeolite modifies the ease of formation of the reaction intermediate directly. When a zeolite impedes formation of a reaction intermediate, the Brønsted–Evans–Polanyi (BEP) principle is likely to apply, so that reaction-intermediate and transition-state shape selectivity occur simultaneously [52]. When a zeolite facilitates formation of a reaction intermediate the BEP principle is likely not to apply [52], so that there can be reaction-intermediate shape selectivity without transition-state shape selectivity.

B Reactant Shape Selectivity If any reactant in a feed is too large to permeate a zeolite this reactant may

References see page 1690

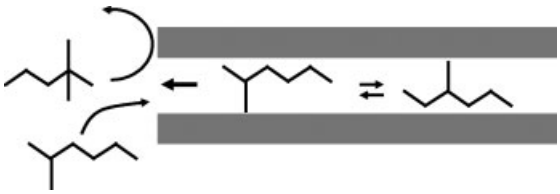

Fig. 4 Reactant shape selectivity. The zeolite leaves the dibranched alkane intact because this isomer is too large to fully permeate into the zeolite pores. Instead, the zeolite selectively transforms the monobranched isomers that can fully adsorb.

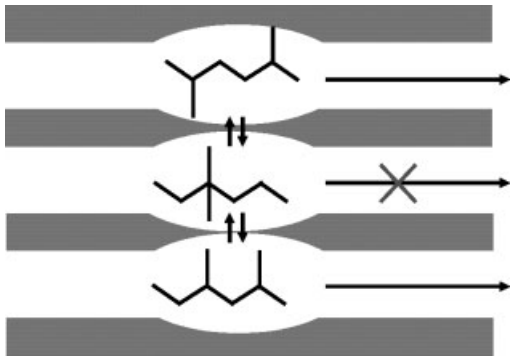

Fig. 5 Product shape selectivity. The zeolite does not contribute any geminal dibranched isomers to the product slate because these isomers react much more rapidly than they desorb. Therefore, geminal dibranched isomers cannot leave the zeolite intact. Instead, the zeolite selectively yields products that can desorb rapidly.

reach the product slate virtually intact. This would be an extreme form of *reactant shape selectivity* (see Fig. 4) [57], in which only those reactants undergo catalytic reactions that can fully adsorb so as to form reaction intermediates, convert, and desorb as products. In general, reactant shape selectivity occurs when reactant conversion is inversely proportional to the extent they exhibit mass transfer limitations. Accordingly, the reactants that adsorb with the smallest mass transfer limitation will be converted most and will be the least prevalent in the product slate.

An example of reactant shape selectivity is the selective combustion of exclusively the linear isomers from a mixture of branched and linear butanes and butenes on Pt-loaded, Ca,Na-exchanged LTA-type zeolite [57]. Whereas, these early experiments involved reactants that are categorically excluded from the LTA-type zeolite pores [57], later experiments included reactants that are excluded by different degrees and, therefore, focused at differences in mass transfer rates as a dominant cause for reactant shape selectivity [58].

C Product Shape Selectivity If reaction intermediates are too large to desorb intact from a zeolite, only their consecutive reaction products can end up in the product slate. This would be an extreme form of *product shape selectivity* (Fig. 5). In general, product shape selectivity occurs when some reaction intermediates exhibit higher mass transfer limitations than others, so that they remain in the adsorbed phase and continue to react for a longer period of time than other, less mass transfer-limited reaction intermediates. Accordingly, the products that desorb with the smallest mass transfer limitation will be the most prevalent in the product slate.

A typical example of this form of shape selectivity is the cracking of hexane isomers in Ca-exchanged LTA-type zeolites [6]. This process yields only linear and no branched cracking products, because only the former can desorb from the zeolite pores.

D Exterior Surface Shape Selectivity In some instances the exterior surface of zeolites process reactants that are either too large to adsorb completely [26] or diffuse too slowly [11–13] to fully permeate the adsorbate. Whether the exterior zeolite surface has a sufficiently regular structure to yield product distributions different from amorphous aluminosilicates remains a subject of debate. In reflecting the lack of agreement on the relevance of the exterior surface to shape selective catalysis, the process has been given a plethora of names, including pore mouth catalysis [11], key-lock mechanism [19, 20], nest-effect [5, 14], and exterior surface shape selectivity [14].

E Other Forms of Shape Selectivity In the previous sections we have listed some of the published mechanisms for shape selectivity. Within the literature, many other types of shape selectivity can be identified, including the ''concentration'' or ''solvent effect'' [59–63], the ''confinement'' or ''solvent effect'' [64–67], molecular traffic control [28, 29], secondary shape selectivity [27], inverse shape selectivity [32], and the ''cage'' or ''window effect'' [23, 24].

5.5.3.3 Molecular Simulations

At this point it is important to recall that the mechanisms described in the previous section are based on the product distribution observed in the desorbed (often gas) phase. Comparatively little is known about the thermodynamics and diffusion properties of the molecules in the adsorbed phase, even though these molecules determine the product distribution observed in the desorbed phase. Molecular simulation provides an attractive alternative to compute these missing properties. A short review on the main simulation techniques is provided here, but for a more extensive description the reader is referred elsewhere [68].

5.5.3.3.1 **Simulation Techniques** The idea of a molecular simulation is simple – that is, to provide a model in the form of an intermolecular potential that describes the interaction between the molecules adsorbed in the zeolite. This model provides the input for a molecular dynamics simulation or a Monte Carlo simulation from which the corresponding thermodynamic and/or transport properties are obtained. For the successful application of these techniques it is important that the intermolecular potentials give a sufficiently realistic description of the experimental systems, and that the simulation techniques are sufficiently powerful such that, for the molecules of interest, accurate properties can be computed within a reasonable amount of CPU time. As will be demonstrated below, both issues are non-trivial.

A Molecular Dynamics of Adsorbed Molecules Suppose we use a molecular dynamics simulation for a system of N particles for which we solve Newton's equations of motion [69]. If there are no external forces working on the system, the total energy is conserved in a molecular dynamics simulation. We therefore perform a simulation in which the energy, E, number of particles, N, and the volume, V, are imposed. A molecular dynamics simulation therefore samples the microcanonical ensemble [68]. Ideally, the real system should be mimicked as well as possible. If successful, the experimental data would also be reproduced, including the diffusion coefficients. Hence it would also be observed that, for the long-chain hydrocarbons that are of interest to hydrocracking, the diffusion coefficient is so small that the corresponding simulations to obtain reliable statistics become prohibitively long. As a consequence, standard molecular dynamics can only be used for those systems that diffuse sufficiently fast that accurate thermodynamic or transport properties can be obtained.

B Monte Carlo Simulation of Adsorbed Molecules Let us consider the experimental set-up required to measure adsorption isotherms. The aim is to measure the number of adsorbed molecules as a function of the pressure of the gas or liquid that is in contact with the zeolite. Experimentally, the most common system is a zeolite in a container that contains a gas or liquid which is maintained at a constant temperature and pressure (or partial pressure in the case of a mixture). At equilibrium, the adsorbed gas molecules have the same temperature and chemical potential as the molecules in the container. The container can be seen as a reservoir that fixes the temperature and chemical potentials of the adsorbed components. In principle, the experimental set-up could be mimicked by simulating a gas or liquid in contact with a reservoir. However, such a system is not very convenient from a simulation point of view.

This experimental set-up closely resembles the grand-canonical ensemble [68] wherein the temperature, volume, and chemical potentials are imposed. An important advantage of the Monte Carlo technique is that a simulation in the grand-canonical ensemble can be performed. In this situation, the reservoir and zeolite are not in direct physical contact, but the Monte Carlo procedure guarantees that the adsorbed molecules have an equal temperature and chemical potential in both the reservoir and in the zeolite. Hence, periodic boundary conditions can be used for the entire zeolite, and the presence of an interface is avoided. The input of the simulation is temperature and chemical potential of the molecules in the reservoir, and the average number of adsorbed molecules is a result of the simulation. The grand canonical Monte Carlo technique functions best if the acceptance of trial moves by which particles are added or removed is not too low. For atomic fluids, this condition effectively limits the maximum loading in a zeolite at which the method can be used. Although the grand canonical Monte Carlo technique can be applied to simple models of non-spherical molecules, special techniques are required as the method converges very poorly for all but the smallest polyatomic molecules.

Although both molecular dynamics and Monte Carlo are very efficient for atoms or small molecules, for large molecules both methods require significant amounts of CPU time. For example, June et al. [70] studied the relaxation of *n*-butane and *n*-hexane in MFI using molecular dynamics, and concluded that the zeolite slowed down the relaxation of these molecules by several orders of magnitude – the longer the chains, the slower the relaxation. Hence, the CPU requirements increase significantly for MD simulations of these long-chain alkanes. The diffusion coefficients of linear alkanes in MFI are sufficiently high that these can be simulated using MD [71], but for the mono-branched alkanes MD can only be used at very high temperatures [72, 73]. Branched alkanes in MFI preferentially adsorb in the intersections between the zig-zag and straight channels [49], and the diffusion is therefore an activated process in which the molecule jumps from one intersection to another [74].

This very slow diffusion path could be avoided via a Monte Carlo simulation in which a new configuration is generated at a random position in the zeolite. The probability that such a move will be accepted depends on the energy difference between the new and the old configurations. Clearly, if a new position is generated on top of a zeolite atom, the attempt will be rejected. For a chain molecule this implies that none of the atoms

References see page 1690

should overlap with the zeolite atoms. If for methane this probability is 1 out of 1000 attempts, then for ethane this will be of the order 1 out of 10^6, and for *n*-octane 1 out of 10^{24}. The conventional Monte Carlo method is therefore very efficient for noble gases or small molecules, but for long-chain alkanes it is equally inefficient as molecular dynamics.

C Configurational-Bias Monte Carlo Technique The configurational-bias Monte Carlo (CBMC) technique has been developed to make possible the insertion of long-chain molecules in moderately dense liquids. The original configurational-bias Monte Carlo technique has been developed for lattice models [75, 76] and has been extended to continuous models [77]. Here, we show how this method can be used to simulate the adsorption of long-chain hydrocarbons in zeolites. In a CBMC simulation the molecules are not inserted at random but rather are grown atom by atom. This growing process introduces a bias which can be removed exactly by adjusting the acceptance rule [68].

In a CBMC simulation a molecule is grown atom by atom using a method based on an algorithm developed by Rosenbluth and Rosenbluth [78]. In this growing scheme, overlap is avoided with the zeolite atoms, and the corresponding bias is removed exactly by adjusting the acceptance rules [68]. The basic CBMC scheme has been extended to branched molecules [49, 79, 80], cyclic molecules [81, 82], and all-atoms models which explicitly include the hydrogen atom [83, 84]. Several ''tricks'' have been devised to increase the efficiency of a CBMC simulation [85]. Compared to ordinary Monte Carlo simulations, CBMC can be up to 10 orders of magnitude more efficient, which has made these types of simulation for long-chain hydrocarbons possible.

In addition, as the growing step in a CBMC scheme provides information on the free energy of adding a molecule to the system, an important application of CBMC is to compute the free energy of a molecule inside the pores of a zeolite.

D Rare Event Simulations A very small diffusion coefficient often is the result of molecules which are trapped in low (free) energy sites and once in a while ''hop'' from one to another adsorption site. In order to compute a diffusion coefficient reliably, a sufficient number of hops must be observed. Most of the CPU time is, however, spent on molecules that ''wait'' close at an adsorption site until a fluctuation gives them sufficient kinetic energy to take the barrier between adsorption sites. The higher the barrier, the longer the molecules remain trapped and – on the time scale of a molecular dynamics simulation – such hopping becomes a very rare event. Special techniques have been developed to simulate such rare events [68]. The basic idea is to compute the hopping rate in two steps [86, 87]. First, the probability that a molecule can be found on top of the barrier is computed. This calculation is followed by a separate simulation in which the probability is computed that a molecule that starts on top of the barrier ends up in the next adsorption site and does not recross the barrier.

The probability of finding a molecule on top of the barrier can be computed directly from the free energy profile, which is the free energy as a function of the position of the molecule in the zeolite. The second step involves the average time that it takes a molecule to cross the barrier. The simplest approach is to assume that transition state theory (TST) holds. A molecule arriving at the top of the barrier is assumed to be in equilibrium with its surroundings, and as a consequence the velocity distribution is given by the Maxwell distribution corresponding to the temperature of the system. TST assumes that half of the molecules that reach the barrier also cross the barrier. TST theory ignores the possibility that such a particle recrosses the barrier and returns into the cage from which it has originated; this may, for example, be due to collisions with the zeolite atoms. This recrossing can be computed directly from a molecular dynamics simulation in which the molecules start on top of the barrier, and the recrossing probability is computed directly. As this involves a simulation that begins on top of the barrier, it is much faster than simulating the time it takes a molecule to climb the free energy barrier. These rare event methods have been applied to zeolites at low [26, 74, 88–90] and even at high loadings [91].

5.5.3.3.2 **Intermolecular Potentials** Most simulation studies follow the assumptions pioneered by Kiselev and coworkers [92] for the adsorption of non-polar molecules. The zeolite is assumed to be rigid and purely siliceous. The adsorbate–zeolite interactions are dominated by the dispersive interactions with the oxygen atoms of the zeolite. The smaller silicon atoms contribute little to the dispersive interaction, and are taken into account implicitly via the oxygen atoms. Further refinements involve the use of a flexible lattice, or the effect of charges for systems that involve polar or Coulombic interactions [93].

A Zeolite–Zeolite Interactions The starting point here is the crystal structure of the zeolite. (Details of most of these structures can be found on the Internet [38].) In case of a rigid zeolite structure, the crystal structure can be used to generate a simulation box containing the desired number of unit cells of the zeolite crystal. Computer

packages are available to perform this procedure both quickly and conveniently [94].

If a rigid lattice is assumed, there is no need for a model of the zeolite–zeolite interactions. In case a flexible zeolite is essential, a variety of models that describe the zeolite–zeolite interactions have been published, the accuracy of which can partly be assessed via a comparison of the calculated vibrational infrared (IR) spectra with the experimental spectra. These models have been discussed in detail by Demontis and Suffritti [95], and the interested reader is referred to this review for details on these models and further references. In order to limit the CPU requirements of a fully flexible zeolite, methods have been developed in which the normal vibrational modes and harmonic crystal approximation are used [96].

B Adsorbate–Adsorbate Interactions For the simulation of hydrocarbons, a variety of models has been proposed, the most realistic being all-atom models in which both the carbon and hydrogen atoms are considered explicitly. In united-atom models, the CH_3, CH_2, or CH groups are considered as a single atom. From a computational point of view, the united-atom model is more efficient and has fewer parameters to be determined; consequently, most studies use a united-atom model. A comparison of the results of such simulations with experimental data for the adsorption and diffusion shows a satisfactory description of the experimental data. In addition, the scatter in these currently available experimental data makes it very difficult to prove that an all-atom model is essential.

For adsorbate–adsorbate interactions it is convenient to distinguish between the intramolecular and intermolecular interactions. The former group are very important to arrive at a realistic representation of the conformation of the adsorbate molecules. Fortunately, these potentials can be based on quantum chemical or spectroscopic data, and therefore for most molecules these models provide a sufficiently accurate description of the intramolecular interactions. In addition, comparisons of various models of, for example, the torsion or bond-bending, show little influence on the thermodynamic properties, such as the vapor-liquid curve [97]. For the hydrocarbon special force fields, both united-atom and all-atom models have been developed that provide an accurate description of the entire vapor–liquid coexistence curve [80, 81, 84, 97–103].

C Zeolite–Adsorbate Interactions Often, zeolite–adsorbate interaction parameters are obtained from fitting to experimental data, and therefore these parameters depend on which accuracy and type of data are used in the fitting procedure. For example, the parameters obtained from fitting to diffusion coefficients can be different from those fitted to, for example, the heats of adsorption or Henry coefficients.

Beerdsen et al. have shown that a very accurate fitting of the parameters of a united-atom model can be obtained through fitting on experimental isotherms with inflection points [91]. This procedure uniquely determined the adsorbent–adsorbate interaction parameters, and is very sensitive to the size parameter as the inflection points in the isotherms are often related to a subtle interplay between different adsorption sites. Several alternative force fields have been developed that also provide an accurate description of the experimental adsorption isotherms [104, 105].

5.5.3.4 Free Energy Model

In this section, it will be shown that molecular simulations afford computation of the thermodynamic and diffusion properties of the reaction intermediates in the adsorbed phase. Knowledge of these properties of the relevant reaction intermediates affords a reinvestigation of the basic assumptions for kinetic models that had been in vogue for a long time.

5.5.3.4.1 Introduction

In the most general case, a feed mixture of many reactants must be considered. The first step is that these molecules must adsorb; indeed, for a given partial pressure of the various components, the concentration of the molecules depends on the *free energies of adsorption*. In the absence of diffusion limitations, a relatively low free energy of adsorption of a particular feed component implies a high adsorbed phase concentration, which often indicates a high reactivity of this reactant. Once a reactant has been adsorbed and has – by definition – formed a reaction intermediate, it can undergo a sequence of reactions forming various other reaction intermediates. The relative importance of these reaction intermediates depends on their *free energy of formation*. Depending on their relative free energy of formation and adsorption, and depending also on the presence of kinetic barriers to desorption, reaction intermediates will either desorb as a product or will continue to transform into other reaction intermediates.

In the free energy model the free energies of adsorption and free energy of formation play an essential role. The free energies of formation of most molecules are tabulated for the gas phase. If molecules are formed in a zeolite, a contribution of the zeolite must be added to this free energy of formation, and this correction corresponds to the free energy needed to bring a molecule from the gas phase into the zeolite. Both the free energy of formation in

References see page 1690

the adsorbed phase and the free energy of adsorption must be known at reaction conditions. This implies that reaction intermediates do not approach gas-phase thermodynamic equilibrium, but rather adsorbed-phase thermodynamic equilibrium. As was observed using *in-situ* NMR [106], free energy contributions by the zeolite can cause major shifts to the gas-phase equilibrium distribution.

At this point it should be emphasized that, in practice, thermodynamic equilibrium among the reaction intermediates often will not be reached, and other (kinetic) factors contribute to the product distribution. Therefore, this free energy model will provide an *idealized reference*, which can be a useful starting point to further investigate the details of a product distribution.

5.5.3.4.2 **Conventional Shape Selectivity** The traditional definition of shape selectivity is related to the observation that reactants which are too large to fit inside the zeolite pores do not go on to form products, that transition states which are too large to fit inside the pores of zeolites do not form, and that reaction intermediates that are too large to desorb intact continue to undergo consecutive reactions [14]. In the free energy model, a high and positive contribution of a zeolite to the free energy of formation is indicative of a bad fit of a transition state or reaction intermediate. Transition states that fit badly exhibit a high free energy of formation, and therefore will contribute little to the product slate. Similarly, reaction intermediates that fit badly exhibit a high free energy of formation and will therefore maintain a low concentration inside the pores. If a minimal concentration of a reaction intermediate entails a minimal contribution to the desorbed phase depends on the reactivity of the thermodynamically impeded species. Thus, contributions from the highly reactive trimethylalkanes can dominate the hydrocracking product slate [44], even though they have a relatively high free energy of formation [26].

A comparison of *n*-decane hydroconversion on FAU- and TON-type zeolites provides a good illustration of the relevance to conventional shape selectivity of the contributions of the zeolite to free energy of formation of reaction intermediates in the adsorbed phase. Figure 6 shows these contributions for FAU- and TON-type zeolites to selected reaction intermediates in the hydroconversion reaction of n-C_{10}, as discussed in Fig. 1. In FAU, the contribution of the zeolite is relatively small, as the cages of FAU are sufficiently large to accommodate all reaction isomers. For this system gas-phase thermodynamic data are therefore a good approximation. The free energies of formation of alkanes with the same degree of branching are similar, and the resulting ideal Gaussian product distribution is simply determined by the number of pathways that generate a particular reaction intermediate; the product slates obtained on amorphous aluminosilicates [34, 35] and on crystalline aluminosilicates with a FAU-type topology [36, 37] are therefore virtually identical. The TON-type pores are

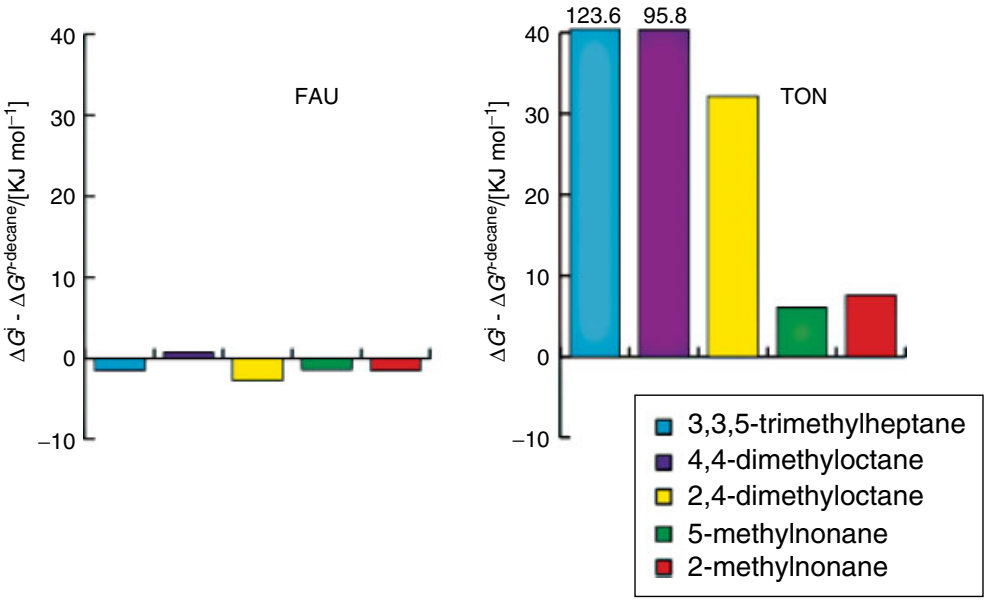

Fig. 6 Contributions of the zeolite to the free energy of formation of typical reaction intermediates in the hydroconversion of *n*-decane. The figure illustrates the free energy difference between the reaction isomer and *n*-decane at $T = 415$ K in the zeolite FAU (left) and TON (right).

much smaller, and the free energy calculations clearly show that this topology inhibits the formation of isomers with proximate branches.

5.5.3.4.3 **Transition-State and Reaction-Intermediate Shape Selectivity** Molecular simulations clearly show that the free energy of formation of alkane isomers with proximate branches are prohibitively high inside TON-type zeolites (Fig. 6), and that – therefore – these isomers will not form in the adsorbed state. Traditionally, the inhibition of formation of these isomers has been attributed to a prohibitively high free energy of formation of the transition state preceding formation of these adsorbed isomers; that is, it has been attributed to kinetic instead of thermodynamic factors [49]. In acid zeolite chemistry this transition state is usually associated with some type of carbocation.

Transition-state selectivity can be defined as a change of free energy of this carbocationic transition state relative to a reaction intermediate as induced by the zeolite framework. Van der Waals interactions between a transition state and the zeolite framework can decelerate the reaction by increasing the free energy of formation of transition states that are incommensurate with the particular zeolite topology [47, 48, 58, 107, 108]. Alternatively, ionic interactions between a transition state and the zeolite framework can accelerate the reaction by decreasing the free energy of formation of transition states that are commensurate with the particular zeolite topology [52]. In order to quantify these effects it is necessary to perform a detailed quantum chemical calculation in the pores of the zeolite, and also to determine the transition state in the pores. These are often very time-consuming calculations and are usually limited to a small region of the zeolite; hence, only a few studies have been published that take the full zeolite structure into account [52]. However, methods are being developed to integrate these quantum chemistry calculations using embedded methods with force field-based methods.

At present, it is not yet feasible to perform a full quantum-chemical calculation to determine unambiguously the free energy of the transition state [109]. However, for many components the BEP relationship holds, which states that the activation energy and reaction energy are related linearly [52–54, 56, 110–112]. Hence, if the zeolite increases the relative free energy of one of the reaction intermediates, the corresponding transition state increases similarly. The consequence of this relationship is that differences in the free energies of the transition states of competing reactions can be estimated from the differences in free energy of formation of the corresponding reaction intermediates (see Fig. 7). If it is assumed that the semi-empirical BEP relationship holds for the entire reaction scheme, it can be deduced which transition states have an increased free energy of formation in the adsorbed state from the computed free energies of the reaction intermediates. A recent suggestion is that the BEP relationship might not hold for instances where adsorbent–adsorbate van der Waals interactions decrease the reaction energy in the adsorbed phase [52]. This would suggest that evaluating the acceleration of reactions due to the zeolite topology-induced facilitated formation of a transition state requires a full-fledged quantum chemical evaluation.

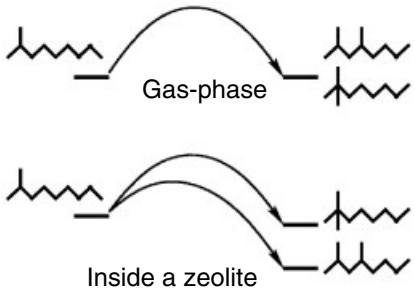

Fig. 7 The Brønsted–Evans–Polanyi (BEP) relationship. In the gas phase the free energies of formation of two products are virtually the same, and so are the free energies of formation of the transition state. In the gas phase, the zeolite increases the free energy of formation of one product relative to that of the other product. According to the semi-empirical BEP relationship, this increases concomitantly the free energy of formation of the transition state for this product – the alkane isomer with geminal methyl groups in this example.

Even if the BEP relationship were always to hold, contributions by the zeolite to either the free energy of formation of the transition state or to the free energy of formation of adsorbed reaction intermediates will result in two distinct forms of shape selectivity [113]. Transition-state shape selectivity will occur irrespective of the presence of diffusion limitations [58], whereas reaction-intermediate shape selectivity will only occur when a reaction is diffusion-limited [114].

Alkane hydroconversion in MFI-type pores provides an illustration of reaction-intermediate shape selectivity. Molecular simulations have shown (see Fig. 8) a large and positive contribution of these zeolites to the free energy of formation of α,α,γ-trimethylalkanes [56]. By comparison, these materials impede the adsorption and formation of α,γ-dimethylalkanes to only a small extent [56]. They do not impede the formation of α,α-dimethylalkanes, monomethylalkanes, and *n*-alkanes, as the shape of these isomers is commensurate with that of the MFI-type intersections, so that all have a similar Gibbs free energy of formation in the adsorbed

References see page 1690

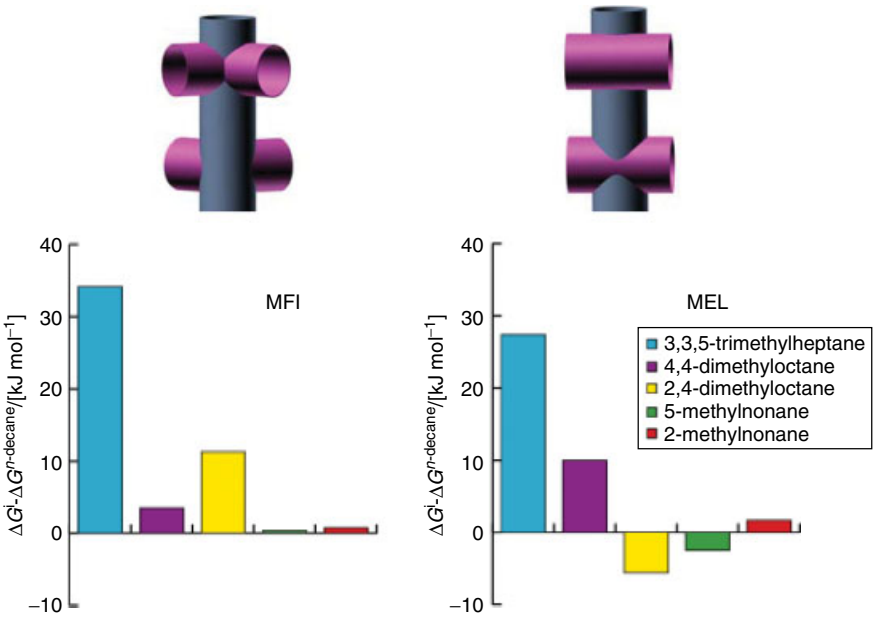

Fig. 8 Comparison of MFI and MEL types of pore. Top: artist's impression of the structures. Bottom: free energies of formation of selected reaction intermediates relative to that of adsorbed *n*-decane.

phase [56]. Accordingly, these free energies indicate that the consecutive hydroisomerization of *n*-alkanes into monomethylalkanes and α,α-dimethylalkanes dominates the shape selectivity in MFI-type pores. Since the favored α,α-dimethylalkanes are hydrocracking precursors which have a low diffusion coefficient, the net result would be that the shape selectivity inside MFI-type pores enhances the hydrocracking rate at the cost of the hydroisomerization rate.

Now, we can compare the product distributions obtained from *n*-decane conversion in MFI- and MEL-type pores. Figure 8 shows that the structures of these two zeolites are very similar; the main difference is that MFI has both sinusoidal and straight channels, whereas MEL has only straight channels. Despite these similarities, the *n*-decane hydrocracking product distribution is very different; the iso-butane yield of MEL is twice that of MFI-type zeolites [56]. Figure 8 shows also that the computed free energies of formation for α,α,γ-trimethylalkanes are highly repulsive, to the extent that their Gibbs free energy of formation in the adsorbed phase effectively prohibits the formation of these hydrocracking precursors in both zeolites. In the absence of α,α,γ-trimethylheptanes, α,α- and α,γ-dimethyloctanes are the most likely hydrocracking precursors [56]. Interestingly, the free energy calculation indicates that α,α-dimethyloctanes have a relatively low free energy at MFI-type intersections, suggesting that these intermediates are commensurate with the shape of the MFI-type intersections, whereas α,γ-dimethyloctanes are commensurate with the shape of one of the MEL-type intersections. Thus, 4,4-dimethyloctane fits snugly when it has its octane backbone in the straight MFI-type channel and the two methyl-groups in the zigzag channel, while 2,4-dimethyloctane has a perfect fit in the large MEL-type intersection because the distance between the two branches matches the distance between the two intersecting channels. The commensurate isomers have the lowest free energy of formation [56]. Due to the relatively large zeolite crystals and high acid site densities used [29, 115], alkanes with the lowest free energy of formation are preferentially formed but cannot diffuse out of the zeolite without being hydrocracked [56]. Since the hydrocracking of 2,4-dimethyloctane yields iso-butane, while hydrocracking of 4,4-dimethyloctane yields *n*-butane, the preferential formation of commensurate isomers suggests an explanation for the twice as high iso-butane yield of MEL- as compared to MFI-type zeolites [56].

This example nicely illustrates the concept of reaction-intermediate shape selectivity; the zeolites preferentially form reaction intermediates that have a low free energy of formation. In the case of MEL- and MFI-type zeolites the important reaction intermediates are those that are commensurate with the zeolite structure and therefore have an unusually low free energy. They can only form at the intersections, for they have a very large free energy at any other position. As a consequence, these molecules cannot diffuse in the pores of the zeolite and are a typical example of ''ship-in-the-bottle'' molecules. So far, these

reactions have only been studied for severely diffusion-limited MFI- and MEL-type zeolite crystals.

As an example of reaction-intermediate shape selectivity induced by adsorbate–adsorbate intermolecular interactions, we can consider the effect of pore size on the hydroisomerization selectivity of the C_6 hydrocracking products formed during *n*-hexadecane hydroconversion. Figure 9 shows that the ratio between the 2,3-dimethylbutane and *n*-hexane yields as a function of pore size forms a bell-shaped curve [26, 30–32, 116]. These results indicate that there exists an optimal pore diameter for the formation of branched alkanes; this phenomenon is often referred to as *inverse shape selectivity* [32], whereby the zeolite is favoring – rather than inhibiting – the formation of the bulkiest isomers, the dibranched alkanes.

This phenomenon was explained in terms of an optimal fit of the branched alkene reaction intermediate with the zeolite pores. However, at low pressures, recent simulations do not reproduce the optimum fit, as was originally reported [114, 116]. At intermediate pressures [117, 118], recent experiments have not reproduced the height of the optimum. Rather, only at high pressures, where adsorbate–adsorbate interactions are important, could such an optimum be reproduced quantitatively [116].

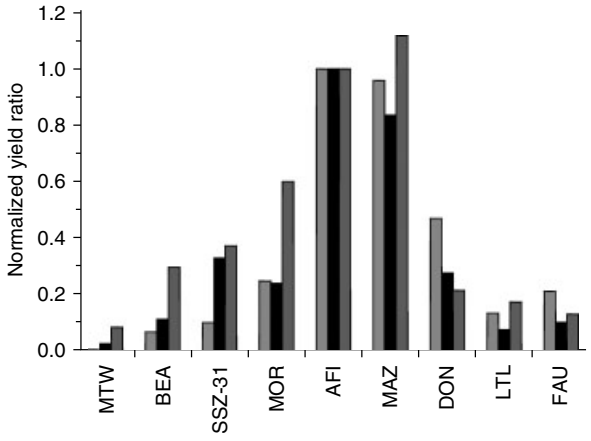

Fig. 9 The effect of pore size on the yield ratio of 2,3-dimethylbutane and *n*-hexane during *n*-C_{16} hydrocracking (increasing pore size from MTW to FAU). So as to facilitate a comparison between simulated (left bar), experimental adsorption ratios (middle bar) and hydroconversion yield ratios (right bar), all ratios were divided by the values obtained for AFI. When the pores are small (as with MTW-type zeolites), repulsive adsorbent–adsorbate van der Waals interactions impede dimethylbutane (DMB) formation; when the pores increase in size these impeding interactions disappear and inter-adsorbent interactions favor formation of the better-packing DMB; when the pore size increases above the 0.74 nm, differences in packing efficiencies disappear because the adsorbents no longer have to line up head-to-tail but can pack in an increasingly more random, liquid-like fashion.

If the pores are too narrow for the bulky dibranched alkane to fit, this will be reflected in a high and positive contribution of the zeolite to the free energy of formation of 2,3-dimethylbutane relative to *n*-hexane. When the pore size increases towards an optimum size, more 2,3-dimethylbutane compared to *n*-hexane can fit in the tubular channels as the dibranched molecule is more compact. Because of these differences in effective size at sufficiently high pressure, the more compact molecule has the lower free energy [26, 116, 119]. This size entropy effect is also responsible for differences in adsorption behavior of these isomers. Figure 9 shows that the tubular MAZ- and AFI-type pores share this optimum size for adsorbing and forming 2,3-dimethylbutane instead of *n*-hexane [116]. When the pores are still larger, the molecules no longer stack linearly so that the adsorbed phase approaches a liquid phase and the entropic size effect vanishes. This difference in packing efficiency leaves its mark on the product slate, because slowly diffusing *n*-C_{16} locks up the initial C_6 hydrocracking products sufficiently long to have them approach adsorbed phase chemical equilibrium. Once desorbed, C_6 is unlikely to compete with C_{16} for adsorption in the zeolite, so that no chemical equilibration towards the gas phase will occur. Thus, severe mass transfer limitations between the gas and adsorbed phases are a prerequisite for this type of reaction-intermediate shape selectivity to occur. In the absence of mass transfer limitations, FAU-, MAZ-, and MOR-type zeolites yield a virtually identical C_6 isomer product slate [120].

Whether the optimum branched isomer yield reported for MAZ- and AFI-type zeolites is indeed only a result of reaction-intermediate shape selectivity remains the subject of debate. Recently, it was suggested that transition-state shape selectivity might also contribute [118]. If there is indeed a contribution, it must be small as an optimized MAZ-type zeolite yields the same yield ratio of 2,3-dimethylbutane and *n*-hexane in the hydrocracking of *n*-hexadecane as do FAU- or MOR-type zeolites [120]. In addition, it was found that 2,3-dimethylbutane diffuses faster than other hexane isomers in MOR- as compared to FAU-type zeolites [121]. If this faster diffusion at high loading for the more efficiently packing molecule can be extrapolated to all topologies mentioned in Fig. 9, then product shape selectivity might contribute to the observed shape selectivity.

5.5.3.4.4 **Reactant Shape Selectivity** Zeolites can shape-selectively process more of one reactant than of another reactant because: (i) the former has a higher diffusion rate; or (ii) the former has a lower *free energy of adsorption*.

References see page 1690

In the former instance of reactant shape selectivity, the reaction needs to be adsorption rate-limited before reactant shape selectivity occurs [58], whereas in the latter instance it is not a prerequisite for shape selectivity. When differences in free energy of adsorption determine the shape selectivity, they do so by affecting the relative concentration of different molecules inside a zeolite. These can be remarkably different from that outside the zeolite. A lower free energy of adsorption is a measure of a higher concentration inside the zeolite, and a higher reactivity. Experimentally, insights into reactant shape selectivity due to differences in free energy of adsorption have been obtained in studies on the chain length-dependence of the reactivity of *n*-alkanes [26, 122, 123], so that the discrimination of zeolites between *n*-alkanes of various lengths depends on the pore topology. To the extent that the reactivity of *n*-alkanes as a function of chain length varies with zeolite topology, it is – by definition [14] – an example of (reactant) shape selectivity.

At low pressure and loading the Henry coefficient is directly proportional to the free energy of adsorption [123, 124]. The Henry coefficient is a measure of the pressure required to adsorb a given amount of molecules in the pores of the zeolite. Most zeolites (such as, FAU- [19, 42], OFF- [125] and MFI- [126] types [122, 127]) are similar to amorphous aluminosilicates, in that the Henry coefficient increases monotonically with the chain length [123]. Hence, a monotonic increase in Henry coefficient with chain length implies a monotonic increase in reactant concentration with chain length. As a result, in the adsorbed phase, the reactivity of *n*-alkanes in hydroconversion increases monotonically with chain length [19]. Accordingly, the products originating from the longer *n*-alkanes dominate the product slate. This selectivity for processing longer alkanes is an example of shape selectivity only in as much as it depends unambiguously on the zeolite pore topology. Figure 10 shows that, for some zeolites, the Henry coefficient decreases as a function of chain length. It is interesting to see how such chain length dependence relates to the chain length-dependence of the *n*-alkane hydroconversion rate of ERI. The ERI-type pore topology exhibits small (diameter ≈0.4 nm) openings (or "windows") providing access to somewhat larger cages [128]. Only from *n*-C_4 to *n*-C_6 ERI-type zeolites exhibit the usual increase in reactivity due to a combination of a lower free energy of adsorption and a higher intrinsic reactivity of the *n*-alkane with chain length [19, 129]. For *n*-alkanes longer than *n*-C_6, hydrocracking diffusion limitations set in [25] and the reactivity becomes increasingly abnormal. Figure 11 shows the chain length dependence of the diffusion coefficient of the *n*-alkanes in ERI. It is apparent that

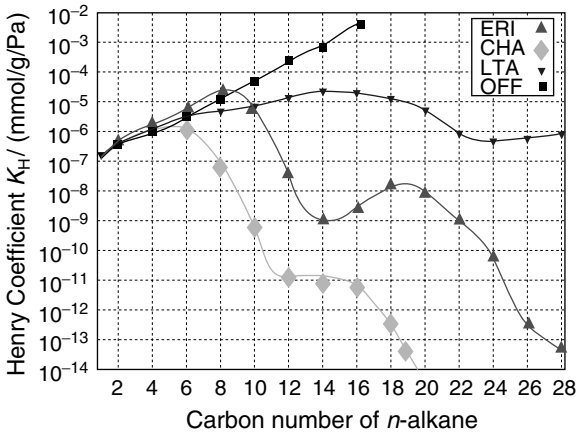

Fig. 10 Henry coefficient as a function of *n*-alkane chain length in various zeolites. When the window size is above a certain diameter (as in OFF-type zeolites), attractive van der Waals interactions between the pore wall and the adsorbed alkane decrease the adsorption enthalpy more than they increase the adsorption entropy; hence, the net effect is a linear decrease in free energy of adsorption (and an exponential increase in Henry coefficient) with increasing *n*-alkane chain length. When the window size is below a certain diameter (as in ERI-type zeolites), repulsive van der Waals interactions between the window and the adsorbed alkane increase the adsorption entropy more than they decrease the adsorption enthalpy, so that the net effect is a linear increase in free energy of adsorption (and an exponential decrease in the Henry coefficient) with increasing *n*-alkane chain length.

diffusion limitations are severe, for they reduce the reactivity from *n*-C_6 to *n*-C_8 [25], and thereby offset both an increase in intrinsic reactivity [19, 26] and a decrease in free energy of adsorption [26]. A similar reduction in reactivity has been reported only once for FER-type zeolites [130].

Surprisingly, the monotonic decrease in reactivity with *n*-alkane chain length in ERI-type zeolites is interrupted at *n*-C_{10}, for *n*-C_{10} is more reactive than *n*-C_8 [25]. Figure 11 shows that this increase correlates well with an increase in diffusion rate [26], suggesting that the strong diffusion limitations remain the dominant cause for changes in reactivity from *n*-C_6 to *n*-C_{10}. Interestingly, molecular simulations fully support the traditional model, which postulates that diffusion rates are the cause for both the decrease and the increase in reactivity. For *n*-alkanes longer than *n*-C_{10}, the reactivity as a function of *n*-alkane chain length changes direction again and now decreases monotonically with the *n*-alkane chain length. This cannot be related exclusively to changes in the diffusion rates, for both experimental and simulated diffusion data indicate that the diffusion rates are still increasing with increasing *n*-alkane chain length and do not peak before *n*-C_{12}–*n*-C_{13} [26]. Only when considering both the simulated non-monotonic variation in Henry

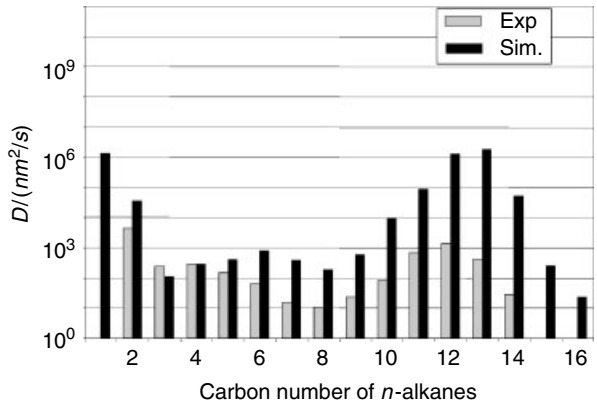

Fig. 11 Diffusion coefficients (experiments: gray = experimental results [24]; black = simulations) in ERI as a function of chain length at 600 K. Due to the high density of windows with a repulsive van der Waals energy between the *n*-alkane and the window in ERI-type zeolites, the diffusion rates in the ERI-type zeolites are several orders of magnitude smaller than those in MFI-type.

coefficient and the simulated non-monotonic variation in diffusion coefficient with *n*-alkane chain length can the experimentally reported monotonic decrease in reactivity with *n*-alkane chain length from *n*-C_{10} to *n*-C_{16} be reproduced [123]. A fully quantitative comparison is difficult due to the likely onset of catalysis at the exterior surface of the ERI-type crystals [123].

5.5.3.4.5 **Product Shape Selectivity** Zeolites can, in a shape-selective manner, yield more of one product than of another product because: (i) the former has a higher diffusion rate; or (ii) the former has a higher free energy of adsorption. In (i), the reaction needs to be desorption rate-limited before product shape selectivity occurs [58], while in (ii) desorption rate limitation is not a prerequisite for shape selectivity. In both cases the zeolite yields more of a particular product because such a product desorbs faster than other products and therefore escapes the reaction cycle at a relatively early stage.

An example of the preferential formation of products that combine the highest free energy of adsorption with the lowest free energy barrier to diffusion (product shape selectivity) is the product isomer distribution observed in *n*-alkane hydroconversion on TON-type zeolites. Recent experimental [42] and simulated [49–52, 73, 131, 132] adsorption data are in agreement that both linear and monobranched alkanes can fully adsorb into TON-type zeolite pores. Experimental [55] and simulation [49] methods also agree that dibranched alkanes with geminal dimethyl groups cannot adsorb in TON-type zeolite pores. By extension, dimethylalkanes should also adsorb into TON-type pores, provided that the methyl groups are far enough apart. However, closer scrutiny reveals that dimethylalkanes can be divided into two groups: those that are commensurate with the periodicity of the TON-type zeolite wall; and those that are incommensurate. The commensurate dimethylalkanes combine a low free energy of adsorption with a high free energy barrier to diffusion, whereas the incommensurate molecules combine a high free energy of adsorption with a low free energy barrier to diffusion [56]. Therefore, only the latter type of dimethylalkanes are found in the hydrocracking product slate [56, 133]. However, this nice example of the importance of the Frenkel–Kontorowa effect to catalysis remains the subject of debate [22, 56].

5.5.3.5 **Concluding Remarks**

The results of these studies have demonstrated the importance of a proper knowledge of the thermodynamic and transport properties of molecules adsorbed in zeolites at reaction conditions. As experiments at these conditions are very difficult to perform, molecular simulations offer an attractive alternative. In particular, as recent developments in novel simulation techniques and force field have allowed for computing these properties to a sufficient degree of accuracy, they may be considered as a good alternative for real experimental data.

It is proposed that shape selectivity be analyzed using a simple concept based on the contribution of the zeolite on the free energies of formation – that is, the free energy of transferring a molecule from the gas phase into the zeolite. The lower this contribution to the free energy, the greater the probability that these molecules are formed as reaction intermediates in the pores of the zeolite. Depending on the diffusion coefficient, these reaction intermediates may leave the zeolite to become products, or they may continue to react. In a similar context, understanding the contribution of the zeolite to the free energies of adsorption of the reactants, provides us with direct information on the contribution of the zeolites to the reaction rates.

We show, by re-examining some well-known examples of various forms of shape selectivity that, once the contributions of the zeolites to the relative free energies of the reaction intermediates are known, a very different explanation of shape selectivity becomes apparent compared to that observed experimentally.

Acknowledgments

As this chapter summarizes the work of many, the authors are especially indebted to Edith Beerdsen, David Dubbeldam, R. Krishna, Bei Liu, Sofia Calero, Martijn Schenk, and Thijs Vlugt. These studies were funded in

References see page 1690

part by the EC through the Marie Curie EXT project MEXT-CT-2005–023311.

References

1. P. M. M. Blauwhoff, J. W. Gosselink, E. P. Kieffer, S. T. Sie, W. H. J. Stork, in *Catalysis and Zeolites*, J. Weitkamp, L. Puppe (Eds.), Springer, Berlin, 1999, pp. 437.
2. K. Tanabe, W. F. Holderich, *Appl. Cat. A: General* **1999**, *181*, 399.
3. C. R. Marcilly, *Top. Catal.* **2000**, *13*, 357.
4. R. H. Jensen, in *Catalytic Science Series*, M. Guisnet, J.-P. Gilson (Eds.), Imperial College Press, London, 2002, Vol. 3, pp. 75.
5. T. F. Degnan, *J. Catal.* **2003**, *216*, 32.
6. P. B. Weisz, V. J. Frilette, *J. Phys. Chem.* **1960**, *64*, 382.
7. P. B. Weisz, *Chem. Tech.* **1973**, *3*, 498.
8. P. B. Weisz, *Pure Appl. Chem.* **1980**, *52*, 2091.
9. P. B. Weisz, *Microporous Mesoporous Mater.* **2000**, *35–36*, 1.
10. P. B. Venuto, in *Molecular Sieve Zeolites-II*, R. Gould (Ed.), Advances in Chemistry Series, American Chemical Society, Washington, DC, 1971, Vol. 102, pp. 260.
11. C. N. Satterfield, J. R. Katzer, W. R. Vieth, *Ind. Eng. Chem., Fundam.* **1971**, *10*, 478.
12. J. C. Cheng, T. F. Degnan, J. S. Beck, Y. Y. Huang, M. Kalyanaraman, J. A. Kowalski, C. A. Loehr, D. N. Mazzone, in *Science and Technology in Catalysis 1998*, H. Hattori, K. Otsuka (Eds.), *Studies in Surface Science and Catalysis*, Elsevier, Amsterdam, 1999, Vol. 121, pp. 53.
13. G. Sastre, C. R. A. Catlow, A. Corma, *J. Phys. Chem. B* **1999**, *103*, 5187.
14. J. Weitkamp, S. Ernst, L. Puppe, in *Catalysis and Zeolites - Fundamentals and Applications*, J. Weitkamp, L. Puppe (Eds.), Springer, Berlin, 1999, pp. 327.
15. E. G. Derouane, *J. Catal.* **1986**, *100*, 541.
16. J. A. Martens, R. Parton, L. Uytterhoeven, P. A. Jacobs, G. F. Froment, *App. Catal.* **1991**, *76*, 95.
17. J. A. Martens, P. A. Jacobs, in *Zeolite Microporous Solids: Synthesis, Structures, and Reactivity*, E. G. Derouane, F. Lemos, F. R. Naccache, F. R. Ribeiro (Eds.), *NATO ASI Series, Series C: Mathematical and Physical Sciences*, Kluwer Academic Publishers, Dordrecht, 1992, Vol. 352, pp. 511.
18. L. C. S. Narasimhan, J. W. Thybaut, G. B. Marin, J. A. Martens, J. F. Denayer, G. V. Baron, *J. Catal.* **2003**, *218*, 135.
19. J. F. Denayer, G. V. Baron, W. Souverijns, J. A. Martens, P. A. Jacobs, *Ind. Eng. Chem. Res.* **1997**, *36*, 3242.
20. W. Souverijns, J. A. Martens, G. F. Froment, P. A. Jacobs, *J. Catal.* **1998**, *174*, 177.
21. M. C. Claude, J. A. Martens, *J. Catal.* **2000**, *190*, 39.
22. M. C. Claude, G. Vanbutsele, J. A. Martens, *J. Catal.* **2001**, *203*, 213.
23. N. Y. Chen, S. J. Lucki, E. B. Mower, *J. Catal.* **1969**, *13*, 331.
24. R. L. Gorring, *J. Catal.* **1973**, *31*, 13.
25. N. Y. Chen, W. E. Garwood, in *Proceedings of the Third International Conference on Molecular Sieves*, J. Uytterhoeven (Ed.), Leuven University Press, Leuven, 1973, Vol. 121, pp. 575.
26. D. Dubbeldam, S. Calero, T. L. M. Maesen, B. Smit, *Angew. Chem.* **2003**, *42*, 3624.
27. D. S. Santilli, S. I. Zones, *Catal. Lett.* **1990**, *7*, 383.
28. E. G. Derouane, Z. Gabelica, *J. Catal.* **1980**, *65*, 486.
29. E. G. Derouane, *J. Catal.* **1981**, *72*, 177.
30. R. A. Van Nordstrand, D. S. Santilli, S. I. Zones, in *Perspectives in Molecular Sieve Science*, W. H. Flank, T. E. Whyte, Jr. (Eds.), ACS Symposium Series, American Chemical Society, Washington, D.C., 1988, Vol. 368, pp. 236.
31. R. A. Van Nordstrand, D. S. Santilli, S. I. Zones, *Synth. Microporous Mater.* **1992**, *1*, 373.
32. D. S. Santilli, T. V. Harris, S. I. Zones, *Microporous Mater.* **1993**, *1*, 329.
33. G. A. Mills, H. Heinemann, T. H. Milliken, A. G. Oblad, *Ind. Eng. Chem.* **1953**, *45*, 134.
34. P. B. Weisz, in *Advances in Catalysis and Related Subjects*, D. D. Eley, P. W. Selwood, P. B. Weisz (Eds.), Academic Press, New York, 1962, Vol. 13, pp. 137.
35. H. L. Coonradt, W. E. Garwood, *Ind. Eng. Chem.* **1964**, *3*, 38.
36. J. Weitkamp, in *Hydrocracking and Hydrotreating*, J. W. Ward, S. A. Qader (Eds.), ACS Symposium Series, American Chemical Society, Washington, D.C., 1975, Vol. 20, pp. 1.
37. J. Weitkamp, *Erdoel Kohle, Erdgas, Petrochem.* **1978**, *31*, 13.
38. F. Alvarez, F. R. Ribeiro, G. Perot, C. Thomazeau, M. Guisnet, *J. Catal.* **1996**, *162*, 179.
39. G. F. Froment, *Catal. Today* **1987**, *1*, 455.
40. G. Martens, G. F. Froment, in *Reaction Kinetics and the Development of Catalytic Processes*, G. F. Froment, K. C. Waugh (Eds.), *Studies in Surface Science and Catalysis*, Elsevier, Amsterdam, 1999, Vol. 122, pp. 333.
41. J. W. Thybaut, G. B. Marin, G. V. Baron, P. A. Jacobs, J. A. Martens, *J. Catal.* **2001**, *202*, 324.
42. J. F. Denayer, A. R. Ocakoglu, W. Huybrechts, J. A. Martens, J. W. Thybaut, G. B. Marin, G. V. Baron, *Chem. Commun.* **2003**, 1880.
43. J. Weitkamp, S. Ernst, in *Guidelines for Mastering the Properties of Molecular Sieves*, D. Barthomeuf, E. G. Derouane, W. F. Hölderich (Eds.), *NATO ASI Series, Series B: Physics*, Plenum Press, New York, 1990, Vol. 221, pp. 343.
44. M. M. Olken, J. M. Garces, in *Proceedings from the Ninth International Zeolite Conference*, R. von Ballmoss, J. B. Higgins, M. M. J. Treacy (Eds.), Butterworth-Heinemann, Boston, 1993, Vol. 2, pp. 559.
45. F. E. Condon, in *Catalysis*, P. H. Emmett (Ed.), Reinhold, New York, 1958, Vol. 6, pp. 43.
46. D. M. Brouwer, H. Hogeveen, *Prog. Phys. Org. Chem.* **1972**, *9*, 179.
47. S. M. Csicsery, *Zeolites* **1984**, *4*, 202.
48. S. M. Csicsery, *Chemistry in Britain* **1985**, *21*, 473.
49. T. L. M. Maesen, M. Schenk, T. J. H. Vlugt, J. P. de Jonge, B. Smit, *J. Catal.* **1999**, *188*, 403.
50. P. Raybaud, A. Patrigeon, H. Toulhoat, *J. Catal.* **2001**, *197*, 98.
51. G. Sastre, A. Chica, A. Corma, *J. Catal.* **2000**, *195*, 227.
52. T. Demuth, X. Rozanska, L. Benco, J. Hafner, R. A. van Santen, H. Toulhoat, *J. Catal.* **2003**, *214*, 68.
53. N. Brønsted, *Chem. Rev.* **1928**, *5*, 231.
54. M. G. Evans, M. Polanyi, *Trans. Faraday Soc.* **1938**, *34*, 11.
55. J. A. Z. Pieterse, S. Veefkind-Reyes, K. Seshan, J. A. Lercher, *J. Phys. Chem. B* **2000**, *104*, 5715.
56. T. L. M. Maesen, M. Schenk, T. J. H. Vlugt, B. Smit, *J. Catal.* **2001**, *203*, 281.
57. P. B. Weisz, *Erdoel Kohle* **1965**, *18*, 525.
58. W. O. Haag, R. M. Lago, P. B. Weisz, *Faraday Discuss.* **1981**, *72*, 317.
59. M. L. Poutsma, S. R. Schaffer, *J. Phys. Chem.* **1973**, *77*, 158.
60. J. A. Rabo, *Catal. Rev. – Sci. Eng.* **1981**, *23*, 293.

61. J. A. Rabo, in *Proceedings from the Sixth International Zeolite Conference*, D. Olson, A. Bisio (Eds.), Butterworth, Guildford, 1984, pp. 41.
62. J. A. Rabo, in *New directions in molecular sieve science and technology*, J. Basset (Ed.), *NATO ASI Series, Series C: Mathematical and Physical Sciences*, Kluwer Academic Publishers, Dordrecht, 1988, Vol. 231, pp. 245.
63. J. A. Rabo, R. D. Bezman, M. L. Poutsma, *Acta Phys. Chem.* **1978**, *24*, 39.
64. E. G. Derouane, *J. Mol. Catal. A: Chemical* **1998**, *134*, 29.
65. E. G. Derouane, *NATO ASI Series, Series B: Physics* **1990**, *221*, 225.
66. E. G. Derouane, J. B. Nagy, *Appl. Catal.* **1989**, *52*, 169.
67. E. G. Derouane, J. B. Nagy, C. Fernandez, Z. Gabelica, E. Laurent, P. Maljean, *Appl. Catal.* **1988**, *40*, L1.
68. D. Frenkel, B. Smit, *Understanding Molecular Simulations: from Algorithms to Applications*, 2nd edn. Academic Press, San Diego, 2002,
69. M. P. Allen, D. J. Tildesley, *Computer Simulation of Liquids*, Clarendon Press, Oxford, 1987.
70. R. L. June, A. T. Bell, D. N. Theodorou, *J. Phys. Chem.* **1992**, *96*, 1051.
71. R. C. Runnebaum, E. J. Maginn, *J. Phys. Chem. B* **1997**, *101*, 6394.
72. D. Schuring, A. P. J. Jansen, R. A. van Santen, *J. Phys. Chem. B* **2000**, *104*, 941.
73. E. B. Webb, G. S. Grest, M. Mondello, *J. Phys. Chem. B* **1999**, *103*, 4949.
74. T. R. Forester, W. Smith, *J. Chem. Soc., Faraday Trans.* **1997**, *93*, 3249.
75. J. Harris, S. A. Rice, *J. Chem. Phys.* **1988**, *88*, 1298.
76. J. I. Siepmann, D. Frenkel, *Mol. Phys.* **1992**, *75*, 59.
77. D. Frenkel, G. C. A. M. Mooij, B. Smit, *J. Phys.: Condens. Matter* **1992**, *4*, 3053.
78. M. N. Rosenbluth, A. W. Rosenbluth, *J. Chem. Phys.* **1955**, *23*, 356.
79. M. Dijkstra, *J. Chem. Phys.* **1997**, *107*, 3277.
80. M. G. Martin, J. I. Siepmann, *J. Phys. Chem. B* **1999**, *103*, 4508.
81. C. D. Wick, M. G. Martin, J. I. Siepmann, *J. Phys. Chem. B* **2000**, *104*, 8008.
82. Z. Chen, F. A. Escobedo, *J. Chem. Phys.* **2000**, *113*, 11382.
83. M. D. Macedonia, E. J. Maginn, *Mol. Phys.* **1999**, *96*, 1375.
84. B. Chen, J. I. Siepmann, *J. Phys. Chem. B* **1999**, *103*, 5370.
85. T. J. H. Vlugt, M. G. Martin, B. Smit, J. I. Siepmann, R. Krishna, *Mol. Phys.* **1998**, *94*, 727.
86. C. H. Bennett, in *Algorithms for chemical computations*, R. E. Christoffersen (Ed.), *ACS Symposium Series*, American Chemical Society, Washington, DC, 1977, pp. 63.
87. D. Chandler, *J. Chem. Phys.* **1978**, *68*, 2959.
88. D. Dubbeldam, E. Beerdsen, T. J. H. Vlugt, B. Smit, *J. Chem. Phys.* **2005**, *122*.
89. F. Jousse, S. M. Auerbach, *J. Chem. Phys.* **1997**, *107*, 9629.
90. T. Mosell, G. Schrimpf, J. Brickmann, *J. Phys. Chem. B* **1997**, *101*, 9476.
91. E. Beerdsen, B. Smit, D. Dubbeldam, *Phys. Rev. Lett.* **2004**, *93*, art. no 248301.
92. A. G. Bezus, A. V. Kiselev, A. A. Lopatkin, P. Q. Du, *J. Chem. Soc., Faraday Trans. II* **1978**, *74*, 367.
93. S. Calero, D. Dubbeldam, R. Krishna, B. Smit, T. J. H. Vlugt, J. F. Denayer, J. A. Martens, T. L. M. Maesen, *J. Am. Chem. Soc.* **2004**, *126*, 11377.
94. Cerius2, 2000.
95. P. Demontis, G. B. Suffritti, *Chem. Rev.* **1997**, *97*, 2845.
96. K. T. Thomson, A. V. McCormick, H. T. Davis, *J. Chem. Phys.* **2000**, *112*, 3345.
97. B. Smit, S. Karaborni, J. I. Siepmann, *J. Chem. Phys.* **1995**, *102*, 2126.
98. J. I. Siepmann, S. Karaborni, B. Smit, *Nature* **1993**, *365*, 330.
99. B. Smit, S. Karaborni, J. I. Siepmann, *J. Chem. Phys.* **1998**, *109*, 352.
100. J. I. Siepmann, M. G. Martin, C. J. Mundy, M. L. Klein, *Mol. Phys.* **1997**, *90*, 687.
101. B. Chen, J. J. Potoff, J. I. Siepmann, *J. Phys. Chem. B* **2001**, *105*, 3093.
102. M. G. Martin, J. I. Siepmann, *J. Phys. Chem. B* **1998**, *102*, 2569.
103. S. K. Nath, F. A. Escobedo, J. J. d. Pablo, *J. Chem. Phys.* **1998**, *108*, 9905.
104. P. Pascual, P. Ungerer, B. Tavitian, A. Boutin, *J. Phys. Chem. B* **2004**, *108*, 393.
105. P. Pascual, P. Ungerer, B. Tavitian, P. Pernot, A. Boutin, *Phys. Chem. Chem. Phys.* **2003**, *5*, 3684.
106. M. W. Anderson, J. Klinowski, *Nature* **1989**, *339*, 200.
107. S. M. Csicsery, in *Zeolite Chemistry and Catalyses*, J. A. Rabo (Ed.), *ACS Monograph*, American Chemical Society, Washington. D.C., 1976, Vol. 171, pp. 680.
108. S. M. Csicsery, *Pure Appl. Chem.* **1986**, *58*, 841.
109. X. Rozanska, L. A. M. M. Barbosa, R. A. van Santen, *J. Phys. Chem. B* **2005**, *109*, 2203.
110. N. Bronsted, *Trans. Faraday Soc.* **1928**, *712*, 726.
111. J. K. Norskov, T. Bligaard, A. Logadottir, S. Bahn, L. B. Hansen, M. Bollinger, H. Bengaard, B. Hammer, Z. Sljivancanin, M. Mavrikakis, Y. Xu, S. Dahl, C. J. H. Jacobsen, *J. Catal.* **2002**, *209*, 275.
112. X. Rozanska, R. A. van Santen, in *Computer Modelling of Microporous Materials*, C. R. A. Catlow, R. A. van Santen, B. Smit (Eds.), Elsevier, Amsterdam, 2004, pp. 165.
113. L. A. Clark, M. Sierka, J. Sauer, *J. Am. Chem. Soc.* **2004**, *126*, 936.
114. M. Schenk, S. Calero, T. L. M. Maesen, T. J. H. Vlugt, L. L. van Benthem, M. G. Verbeek, B. Schnell, B. Smit, *J. Catal.* **2003**, *214*, 88.
115. J. Weitkamp, P. A. Jacobs, J. A. Martens, *Appl. Catal.* **1983**, *8*, 123.
116. M. Schenk, S. Calero, T. L. M. Maesen, L. L. Van Benthem, M. G. Verbeek, B. Smit, *Angew. Chem.* **2002**, *41*, 2499.
117. B. L. Newalkar, R. V. Jasra, V. Kamath, S. G. T. Bhat, *Adsorption* **1999**, *5*, 345.
118. J. F. M. Denayer, A. R. Ocakoglu, J. A. Martens, G. V. Baron, *J. Catal.* **2004**, *226*, 240.
119. J. Talbot, *AIChE J.* **1997**, *43*, 2471.
120. S. Calero, M. Schenk, D. Dubbeldam, T. L. M. Maesen, B. Smit, *J. Catal.* **2004**, *228*, 121.
121. J. M. van Baten, R. Krishna, *Microporous Mesoporous Mater.* **2005**, *84*, 179.
122. A. Jentys, J. A. Lercher, in *Introduction to Zeolite Science and Practice*, H. van Bekkum, P. A. Jacobs, E. M. Flanigen, J. C. Jansen (Eds.), *Studies in Surface Science and Catalysis*, Elsevier, Amsterdam, 2001, Vol. 137, pp. 345.
123. T. L. M. Maesen, E. Beerdsen, S. Calero, D. Dubbeldam, B. Smit, *J. Catal.* **2006**, *237*, 278.
124. D. Dubbeldam, S. Calero, T. J. H. Vlugt, R. Krishna, T. L. M. Maesen, B. Smit, *J. Phys. Chem. B* **2004**, *108*, 12301
125. N. Y. Chen, J. L. Schlenker, W. E. Garwood, G. T. Kokotailo, *J. Catal.* **1984**, *86*, 24.
126. J. Wei, *Chem. Eng. Sci.* **1996**, *51*, 2995.

127. J. A. Lercher, K. Seshan, *Curr. Opin. Solid State Mater. Sci.* **1997**, *2*, 57.
128. C. Baerlocher, W. M. Meier, D. H. Olson, *Atlas of Zeolite Framework Types*, 2001, p. 1.
129. J. F. Denayer, G. V. Baron, P. A. Jacobs, J. A. Martens, *Phys. Chem. Chem. Phys.* **2000**, *2*, 1007.
130. J. P. Giannetti, A. J. Perrotta, *Ind. Eng. Chem.* **1975**, *14*, 86.
131. E. B. Webb, III, G. S. Grest, *Catal. Lett.* **1998**, *56*, 95.
132. L. Domokos, L. Lefferts, K. Seshan, J. A. Lercher, *J. Catal.* **2001**, *203*, 351.
133. J. A. Martens, W. Souverijns, W. Verrelst, R. Parton, G. F. Froment, P. A. Jacobs, *Angew. Chem.* **1995**, *34*, 2528.